NMR Relaxation and Self-Diffusion Study at High and Low Magnetic Fields of Ionic Association in Protic Ionic Liquids

Geoffrey L. Burrell,[†] Iko M. Burgar,[‡] Qingxia Gong,[§] Noel F. Dunlop,[||] and Frances Separovic*[,†]

The University of Melbourne, Melbourne, VIC 3031, Australia, CSIRO Materials Science & Engineering, Clayton, VIC 3169, Australia, RWTH Aachen University, D-52056 Aachen, Germany, and Orica Ltd., Melbourne, VIC 3002, Australia

Received: June 3, 2010; Revised Manuscript Received: August 4, 2010

NMR relaxation and diffusion characterization of several protic ionic liquids at high and low magnetic fields are reported. The dynamics of cations and anions were similar at both frequencies, with similar trends and magnitudes for a fixed component paired with oppositely charged species. An Arrhenius relationship was displayed between the molecular motion and the glass transition temperature. The diffusion of ions showed a strong degree of ion correlation between cation and anion, and Arrhenius plots of relaxation and diffusion indicated that the ions diffused as a pair. At high field diffusion was dominated by mobile species that followed Stokes−Einstein behavior. Conversely, diffusion observed at low field emphasized relatively immobile species that displayed fractional Stokes−Einstein behavior. No evidence was found to indicate the influence of magnetic field on structural and dynamic properties of the studied ILs; however, variation between diffusion coefficients at different magnetic fields indicated dynamic heterogeneities (or temporal aggregates) within the ionic liquid.

Introduction

Ionic liquids (IL) possess a range of unique properties that make them ideal candidates for a variety of applications, e.g., reaction catalysts, novel biomass solvents and high-temperature electrolytes.[1−7] However, there remain several factors that complicate and restrict their development.[8] For example, although composed entirely of ions, ionic liquids are not completely dissociated—some degree of ion association remains present.[9] The ion-pair concept has been long known for concentrated electrolyte solutions and in molten salts,[10−13] and larger associated complexes of ion pairs or ordered ionic networks have also been examined.[14,15] A significant drawback of partial ionic association results in the relatively low and variable diffusivity of the ionic species, which effects the overall viscosity and ionic conductivity.[16]

Ion pairing within IL has been observed at the solid−liquid interface and the gas phase.[17,18] Aggregation in the bulk liquid, however, differs from structure formed at the interface, albeit these studies do provide important insights into liquid phase ordering.[19,20] Molecular dynamics calculations of incompletely dissociated IL in the bulk liquid have indicated the formation of ionic domains.[21] In conventional aprotic IL, the compound can be roughly grouped into two distinct regions: the polar section consisting of anions and cations, and nonpolar section mainly consisting of the attached alkyl chain. The nonpolar alkyl chains form heterogeneous domains that become larger as the length of the alkyl chain increases, while the cation and anion headgroups form interfaces where charges are distributed uniformly.[22,23]

Protic IL (PIL) differ from other types of IL, in that the ionic moiety is formed from the transfer of a proton from a Brønsted acid to a Brønsted base.[24,25] Neutral aggregates of PIL were hypothesized and later directly observed, both in the gas phase and at the PIL−solid interface.[26−28] Simulations of hydrated protons in very concentrated aqueous solutions also indicate long-range order, which is likewise present in the bulk liquid.[29]

Regardless of the ionic constituent, it is generally accepted that there is some degree of association in IL. Ion pairs under suitable conditions may undergo self-aggregation, forming ion quadrupoles or higher aggregates through dipole−dipole interactions.[30,31] Strong charge ordering can lead to long-range order even in the presence of a solute and may arise from the competition among electrostatic, dispersion, and hydrogen-bonding interactions.[32−34]

Pulsed gradient spin echo (PGSE) NMR self-diffusion measurement is an excellent technique for studying ionic diffusion in the solid and liquid state.[35−41] Self-diffusion coefficients obtained from NMR can be useful for detecting dimers and ion pairs or nanoaggregates in the liquid state.[42−45] However, due to dynamic exchange between dissociated ions and hypothetical ion pairs, it is practically impossible to distinguish between ion states (eq 1).[46]

$$D_{obs} = xD_{ion} + (1 - x)D_{pair} \quad (1)$$

where x is the existence probability of the ion and equal to the dissociation degree of the salt.[47] As a result, the observed spectroscopically detected self-diffusion coefficient (D_{obs}) is a contribution from both the associated IL and the dissociated ions.

Additional difficulties in determining diffusion rates can also arise due to the immediate orientation of low-molar-mass liquids in an external field.[48] Recent reports have indicated IL aggregates changing configuration as a result of an external electric field.[49] Application of an electric field increased self-diffusion coefficients by more than an order of magnitude over values from

* Corresponding author. E-mail: fs@unimelb.edu.au.
[†] The University of Melbourne.
[‡] CSIRO Materials Science & Engineering.
[§] RWTH Aachen University.
[||] Orica Ltd.

10.1021/jp105087n
Published on Web 08/16/2010

the equilibrium state without electric field.[50] Similar behavior is observed in liquid crystals that can orient parallel to the direction of the magnetic field.[51,52] Such ion orientation can cause fast ion transport by forming efficient conduction pathways for ionic or molecular species.[53]

Low frequency NMR has been applied to study structural anisotropy as well as domain formation and dissociation processes in complex heterogeneous compounds.[54−56] The technique has been reported for length scales extending up to the order of tens of nanometers, so it has become a useful tool in polymer science.[57,58] Due to the low intensity and low frequency of the magnet field, the chemical shift cannot be used at this low frequency to discriminate the different molecular species. Instead, relaxation times and spin diffusion can be used to identify liquid at the solid−liquid interface and/or an amorphous phase as well as possibly a "solid-like" state.[59]

To examine aggregation in PIL, a comparison between results in a strong and weak magnetic field has been made. Here we present a direct measurement in PIL of ionic mobility, D, at both high field (500 MHz) and low field (18.3 MHz), which showed a disparity that was indicative of ion association.

Experimental Section

Materials and Chemicals. PIL were prepared by the simultaneous addition of dried and freshly distilled acid and base under inert gas into a water-jacketed reactor equipped with a stirrer.[60] Component ratios were determined to be equimolar within 0.1% (mol/mol) from the mass of reagents and confirmed approximately by single pulse ^{1}H NMR. PIL were stored under an inert atmosphere in the dark. Bases used to form cations were diethanolamine ($(HOEt)_2NH$), diethylamine ((Et_2NH)), triethylamine (Et_3N), tributylamine (Bu_{3N}), bis(methoxyethyl)amine ($(MeOEt)_2NH$), pyrrolidine (pyrr). The corresponding anions that gave room temperature PILs were dibutylphosphoric ($(BuO)_2PO_2H$), methanesulfonic (MsOH), sulfamic (OSA), acetic (AcOH), and formic acids (HO_2CH). All other chemicals were obtained from Aldrich (St Louis, MO) and used as received.

Neat liquid PIL samples were transferred under an inert atmosphere to the internal chamber of a Wilmad (Buena, NJ) NMR coaxial capillary insert of volume 60 μL with a solution of 1% (w/w) sodium 3-(trimethylsilyl)propionic acid-d_4 (TSP) in D_2O in the external chamber. The insert was sealed with Parafilm (Alcan Packaging, Neenah, WI), and NMR measurements were carried out immediately. The external D_2O provided a lock frequency, and TSP was used to convert the spectrum reference scale to TMS as 0 ppm. The sample temperature, 298.13 K, was calibrated using the temperature dependent chemical shift of methanol.

Low field NMR data were recorded with a custom built profile NMR-MOUSE spectrometer (18.1 MHz for ^{1}H) with a uniform field gradient in the sensitive region of 22.36 T m^{-1} (RWTH Aachen, Germany).[61] Samples were run neat in 10 mL vials with 15 mm diameter and a minimum sample depth of 10 mm. Multiecho trains were acquired and their amplitudes analyzed in the time domain.

Viscosity values were obtained using a TA Instruments (New Castle, DE) AR-G2 stress-controlled cone and plate rheometer with 4 mm diameter and 2° cone angle under steady flow. Samples were equilibrated at 298 K for 10 min before measurement.[62]

Spin−Lattice and Spin−Spin Relaxation Times. ***High Field.*** The spin−lattice relaxation time (T_1^{HF}) was determined by sampling the amplitude of the FID following the inversion−recovery pulse sequence $\pi-\tau_1-\pi/2$ for 15 values of τ_1. The relaxation delay was set to 10 s, which was always greater than $5T_1^{HF}$. Fitting errors were less than 5%. The spin−spin relaxation time (T_2^{HF}) was similarly obtained by using the Hahn-echo pulse sequence $\pi/2-\tau_2-\pi-\tau_2$.[63]

Low Field. The spin−lattice relaxation times (T_1^{LF}) were determined by sampling the amplitude of the FID following the saturation-recovery pulse sequence $\pi/2-\tau_1-\pi/2$ for 15 values of τ_1 and fit as a single exponential.[63] The relaxation delay was set to 10 s, which was always greater than $5T_1^{LF}$. A diffusive component from the continuously applied high gradients influenced the spin−spin relaxation; hence, the effective spin−spin relaxation (T_{2eff}^{LF}) was fitted as a single component exponential decay using the CPMG pulse sequence $\pi/2-\tau_2/2-(\pi-\tau_2)_x-$, where $\tau_2 = 0.04$ ms and x was between 1000−8000.[63]

Self-Diffusion Coefficients. ***High Field.*** ^{1}H NMR experiments were collected on two instruments. A Varian (Palo Alto, CA) INOVA 500 MHz NMR spectrometer operating at 500.2 MHz for ^{1}H using a 5 mm probe with z-gradient strength of 0.636 T m^{-1}.The dead time of the spectrometer is 4 μs. The length of a $\pi/2$ pulse was about 14 μs, and the recycle delay was 10 s for all measurements. Twenty gradients were applied and linearly increased from 1.5 to 100% maximum gradient strength (g_{max}) with 16 repetitions acquired at each increment. The achieved temperature stability was ±0.1 K. Δ values ranged from 50 to 100 ms, δ was fixed at 4 μs, and the spectral width was ∼16 kHz.

A Bruker (Karlsruhe, Germany) Avance 500 wide bore spectrometer operating at 500.1 MHz for ^{1}H was equipped with a Diff30 gradient probe with a single (i.e., z) shielded gradient coil connected to a GREAT60 current amplifier and capable of achieving pulsed gradients of 17.90 T m^{-1}. A PGSTE pulse sequence containing "half-sine-wave" shaped gradient pulses and a homospoil pulse was used to reduce the sequential pulse mismatch, probe "ringing", and eddy currents.[64] A total of 50 gradient strengths were used in the range 0.30−9.00 m^{-1} with a 10 s recycle delay and 8 repetitions. Δ was fixed at 50 ms, δ was 2.5 μs, and the spectral width was ∼16 kHz.

Pulsed field gradient (PFG) NMR was performed using a PFG stimulated-echo (PGSTE) pulse sequence with a 10 s relaxation delay. Samples were inserted into the probe for at least 30 min prior to diffusion measurements to allow for temperature equilibration. The self-diffusion coefficients (D) of the spin−echo attenuation data, based on the integrals of the ^{1}H resonance, were determined from least-squares fits to the Stejskal−Tanner equation (eq 2)[65]

$$\ln \frac{I}{I_0} = -D\cdot\delta^2\cdot\gamma^2\cdot g^2\cdot\left(\Delta - \frac{\delta}{3}\right) \qquad (2)$$

where I/I_0 is the observed signal intensity. The magnetogyric ratio and the gradient strength are denoted by γ and g, respectively. The width of the gradient pulses is given by δ and the delay between the midpoints of the gradient pulses by Δ. For all studied PIL the observed echo decays were single-exponential and gave excellent fits to eq 2.

Low Field. A steady gradient stimulated echo (SGSTE) was collected in the presence of a steady gradient with a Carr−Purcell−Meiboom−Gill (CPMG) echo train after the main

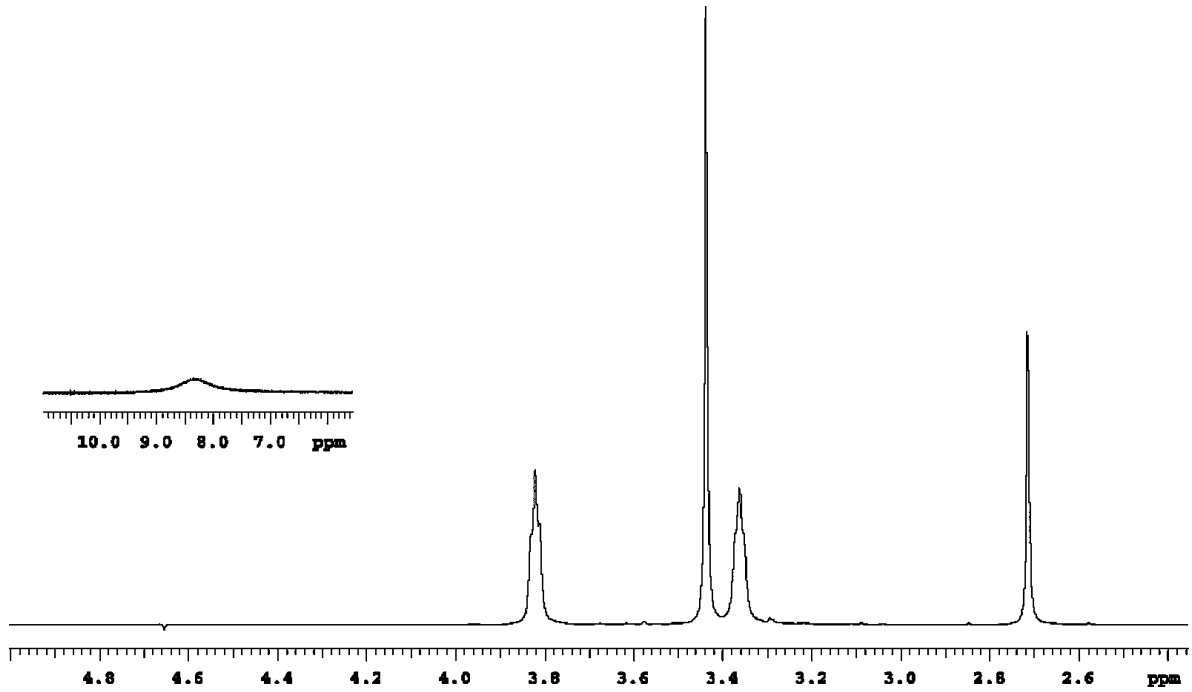

Figure 1. ^{1}H NMR spectrum of $(MeOEt)_2NH\cdot MsOH$ at 298 K. δ_H in ppm (500 MHz, neat, TSP): 3.81 ($-CH_2N$), 3.42 (MeO$-$), 3.28 (OCH_2-), 2.65 (MsOH). Inset: broader resonance of $-$NH and $-$OH protons.

diffusion encoding period by varying the time δ between pulses.[61] Typically, a time of less than 3 min was required to measure a complete diffusion curve. The gradient of the NMR-MOUSE was determined with hexane, ethanol and water.[61] The signal attenuation for the SGSTE is given by eq 3

$$\ln \frac{I}{I_0} \approx -\gamma^2 G^2 {\tau_1}^2 \left(\tau_2 + \frac{2}{3}\tau_1\right) D \qquad (3)$$

where τ_1 is the mean δ noting the time between the first two $\pi/2$ pulses, τ_2 is the time between the latter two $\pi/2$ pulses and the remainder are defined as per eq 2. The τ_1 period was exponentially increased in 20 increments from $\tau_1 = 0.002$ ms until $I/I_0 \approx 0$. The amplitudes of the stimulated echo (eq 3) are attenuated by relaxation processes, primarily the transverse relaxation time T_2. The diffusion terms dominate for large values of D, as is the case for low viscosity liquids and when strong magnetic field gradients are used. The results of Rata et al.[61] show that eq 3 is valid to a good approximation. The CPMG echo train is also attenuated by the diffusion process due to the presence of the strong field gradient but use of a short interecho time delay alleviates this effect. Furthermore, the diffusion encoding of the CPMG echo train remains constant during the variation of the time parameters τ_1 and τ_2 and does not affect the validity of (eq 3).

Results and Discussion

Relaxation Measurements. NMR relaxation measurements provide data about molecular motional dynamics at the atomic level and are sensitive to changes induced by self-association.[66] If lifetimes of a monomer and aggregates are short on the NMR relaxation time scale, observed relaxation rates are a weighted average of the different species present.[67] Even a small amount of high molecular weight species, from a tetramer for example, can cause a significant change in the observed relaxation rates. Thus, measurements and analysis of NMR relaxation data can provide structurally resolved information on self-association that would not be accessible otherwise.

PIL have a high viscosity compared to viscosities of typical NMR solvents, leading to relatively broad NMR line widths, and fine coupling was not readily visible for bis(methoxyethyl)ammonium methanesulfonate ($(MeOEt)_2NH\cdot MsOH$) or the other examined PIL (Figure 1).[68] Broad line widths typically indicate low mobility in the fluid. Protons in $-$OH and $-$NH capable of inter- or intramolecular exchange gave rise to a single downfield signal much broader than the other signals ($\sim$500 Hz versus $\sim$50 Hz), which resulted from an average of chemical environments. The coalescence of resonances occurs when two or more spins are exchanging faster than the frequency difference between two different chemical shifts, representing unique chemical environments. It is known that the base was in the ionized form (ammonium-type nitrogen), but proton exchange between the acid and base or othweer functional groups cannot be dismissed.[60] Despite the line broadening, the PIL appeared to be small molecules with chemical shifts that were easily identified.

For the range of PIL examined, the diverse functional groups could be too different to readily compare against each other. However, for a constant base, $(MeOEt)_2NH$, with three different acids, some comparisons can be made (Figure 2). Fast decay of a signal was caused by the "rigid" or nonflexible hydrogen groups of the matrix, which would be found inside a heterogeneous domain, and the slow decay component was mainly attributed to protons of the mobile molecules not associated with aggregation or interaction.[69,70]

The T_1^{HF} of the three alkoxy chain resonances varied with the combined acid. For the methanesulfonic acid (MsOH) pair, the terminal methoxy group (MeO$-$) had the longest relaxation time and indicated relative mobility in comparison to acetic acid (AcOH) and sulfamic acid (OSA) which were relatively immobile and similar to each other (Figure 2a). The methylene adjacent to the cationic nitrogen ($-CH_2N-$) relaxed faster than the methoxy for both MsOH and AcOH but was slower for the

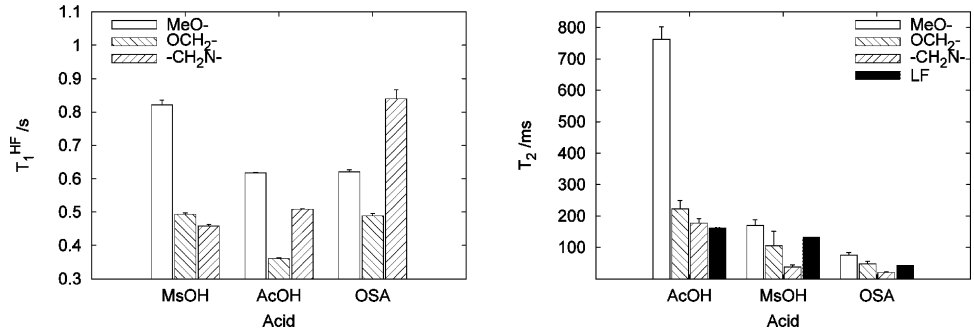

Figure 2. (a) T_1 and (b) T_2 relaxation times of $(MeOEt)_2NH$ with methanesulfonic at 298 K (MsOH, strong acid), acetic (AcOH, moderate acid), and sulfamic acids (OSA, weak acid).

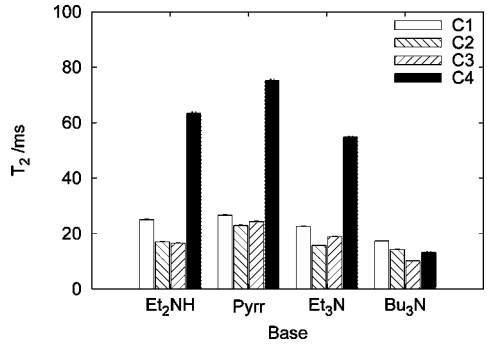

Figure 3. T_2^{HF} relaxation times of $(BuO)_2PO_2H$ with four different bases at 298 K, where C_x denotes the alkyl chain number from phosphate.

OSA pair. The methylene in the "center" of the alkoxy chain (OCH_2-) was approximately constant across the three PIL, indicating that the different acids affected the dynamics of both the ionic nitrogen and the alkoxy tail of base. The factors affecting relaxation rates are diverse and may be the combination of multiple effects (i.e., ion pair distance, conformational changes, chemical shift anisotropy). Hence, comparison of the single value of T_1^{LF} with the individual values for T_1^{HF} would not convey sufficient information for magnetic field reorientation effects.

On the other hand, changes in the magnetic field strength had little impact on T_2 at room temperature. The relaxation times of alkoxy chains of the same $(MeOEt)_2NH$ base varied with increasing distance from the ionic nitrogen (Figure 2b). The MeO− group took longer to relax and was much more mobile than the ethyl chain (OCH_2-, $-CH_2N-$) close to the proton exchange site. The small change between T_2^{LF} and T_2^{HF} indicated that the relaxation rate, $1/T_2$, was in the region of fast reorientational motion and that any observed differences between HF and LF NMR were not due to physical effects of the magnetic field.

To study the relaxation rate variation for a PIL series with a constant acid analogous to the consistent base discussed before, dibutylphosphoric acid, $(BuO)_2PO_2H$, was investigated. For $(BuO)_2PO_2H$ the T_2^{HF} were relatively similar along the length of the alkyl chain, with the exception of the relatively very mobile terminal methyl groups (C_4) (Figure 3). The longer relaxation time for methyl groups of PIL with diethylamine ((Et_2NH)), pyrrolidine (Pyrr), and triethylamine (Et_3N) suggested that the ionic headgroups possessed some degree of order but the alkyl chain were relatively disordered. However, the base Bu_3N induced $(BuO)_2PO_2H$ into a completely rigid chain with comparable T_2^{HF} values for all chain resonances. Such alkyl chain ordering can arise from aggregation of polar and nonpolar domains, and simulations have predicted for other IL when alkyl chains are longer than four carbons.[71]

To further probe the organization of PIL, NMR relaxation rates were investigated over the temperature range from 298 to 353 K (Figure 4). NMR motional narrowing takes place when the fluctuations of the local magnetic fields are comparable with rigid-lattice line widths.[72] This may be due to either exchange interactions resulting from intermolecular collisions (i.e., proton transfer) or dipole−dipole interactions. For ionic interparticle interactions, it has been suggested that it is the time-dependent dipolar interactions that are the dominant relaxation mechanism.[73−75]

As an example compound, the T_1^{HF} of $(MeOEt)_2NH\cdot MsOH$ increased with temperature due to thermal disorder (Figure 4a). The motional process showed Arrhenius-type response to increasing temperature, given by eq 4

$$T_1 = A\cdot e^{E_a/k_B T} \tag{4}$$

where A is a fitting factor, E_a is the activation energy of the narrowing process, and k_B is Boltzmann's constant. T_1 is mostly related to the molecular reorientational motions; hence, the good Arrhenius fitting over the investigated temperature range indicates a single motional mode. The relaxation rates measured at the terminal methoxy (MeO−) were the slowest, closely followed by the methanesulfonic acid methyl group (MsOH). Protons of both acid and base capable of intermolecular exchange were obtained as a single broad average signal, and rates were moderately faster but were intermediate to the fastest moving ethyl chain resonances. The exception to Arrhenius fits was from the methylene closest to the ionic nitrogen ($-CH_2N$), which decreased in T_1^{HF} from 313 K and changed to another state from 323 K that had a temperature response concordant with the other resonances. As $(MeOEt)_2NH\cdot MsOH$ was measured at much higher temperature than the melting point transition at 283 K, as measured by differential scanning calorimetry (Supporting Information), this T_1^{HF} jump was indicative of another unidentified thermally induced phase transition specific to the groups adjacent to the ionic center.

T_2^{HF} values of the acid and base methoxy groups also increased from room temperature to 353 K (Figure 4b). Although the $-CH_2N$ group did not show any T_2^{HF} jump with temperature, the T_2^{HF} of the adjacent ethylmethylene group (OCH_2-) and terminal MeO− decreased at both the high and low end of the temperature range. Changes in T_2^{HF} with temperature likely result from subsequent alteration of the motions of the alkoxy chain, rendering long-range ordering less likely in comparison to short-range ordering once thermal motion began to dominate.

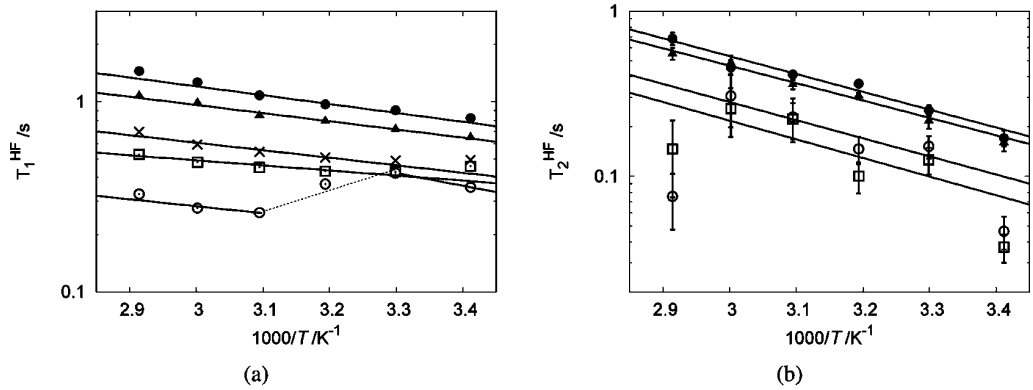

Figure 4. Semilog Arrhenius plots of (a) spin−lattice (T_1) and (b) spin−spin (T_2) relaxation of $MeOEt_2NH \cdot MsOH$ as a function of inverse temperature. Continuous lines arise from Arrhenius fitting. The dotted line is a guide for the eye. Symbols denote the following resonances: exchanging protons (×); MeO− (●); OCH_2− (⊡), $-CH_2N$ (⊙); MsOH (▲).

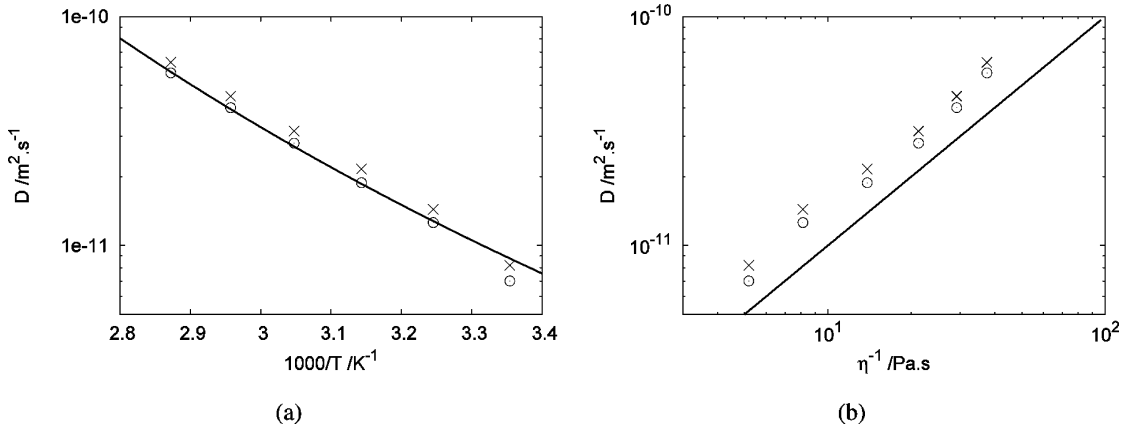

Figure 5. Plots of $(MeOEt)_2NH \cdot MsOH$ cation and anion diffusion constants, D, at 500 MHz: $(MeOEt)_2NH$ (×); MsOH (⊙). Associated errors were smaller than point size. (a) Semilog Arrhenius plot of D as a function of T^{-1} with Arrhenius line fitting, and (b) log−log plot of D as a function of η^{-1}, where the dissimilar sized cation and anion have similar diffusion coefficients regardless of temperature. The indicative line arises from the Stokes−Einstein equation, $D \propto \eta^{-1}$.

While thermal disordering would be expected to give weaker interaction at higher temperature, there may be another factor to be consider: the role of impurities that can come between the pairs (e.g., water molecules). The impurities become more mobile at higher temperature, therefore allowing the IL pairs to settle into the more tightly bound group resulting in the shorter T_2^{HF} (Figure 4b). The sudden jumps in the relaxation times may be due to the different time scales of the motions; observed T_1^{HF} is sensitive to the faster moving molecules (short-range order) while the observed T_2^{HF} is dominated by aggregation (long-range order). Changes in molecular interactions are characterized by alteration of relaxation times, indicating the melting transition of $(MeOEt)_2NH \cdot MsOH$ may correlate to breakdown of aggregate structure.

Diffusion Studies. Unlike relaxation measurements, self-diffusion coefficients (D) at HF were very similar for all resonances of a given molecule; hence, measurements at different magnetic fields were directly comparable. D were about 2 orders of magnitude lower than those measured in conventional organic electrolytes, which is strongly related to the high viscosity of these media.[76]

Due to experimental time limits the majority of experiments were conducted on a 500 MHz instrument with a maximum gradient strength of 0.636. However, at this gradient strength three of the samples could not be measured, as Δ became so long that the relaxation time attenuated the results. Therefore, when samples were found where $\Delta > 0.1T_1$, a separate 500 MHz instrument was used with a larger maximum gradient of 17.90 T m^{-1} that prevented longitudinal relaxation from attenuating the diffusion curves. Control samples run at both gradients showed less than 3% deviation in resultant D values.

The NMR diffusion method was examined in detail with $(MeOEt)_2NH \cdot MsOH$ as there were four distinct NMR resonances: the cation methoxy group and ethyl chain, the anion methyl group, and the single resonance from the exchanging protons of both species. As resonances from a given molecule gave similar results, the comparatively narrow methyl resonances were used for equation fitting. The temperature dependence on D of cation and anion exhibited an Arrhenius relationship over the temperature range examined, as seen for many aprotic IL (Figure 5a).[35,37] Typically, diffusion of species in a solution is related to the molecular size and the medium viscosity. In the case of the observed PILs with $(MeOEt)_2NH \cdot$ **L**MsOH as the given example, despite the cation size being almost twice that of the anion, both molecular species had very similar D regardless of temperature, an observation that has been attributed to ion pairing.[77,78] A log−log plot of D against η^{-1} was approximately linear and showed that both cation and anion followed Stokes−Einstein behavior and, at increased temperature, the similar D indicated a thermally stable ion pair (Figure 5b).

At HF, the measured diffusion coefficient is limited by the short spin−spin relaxation time constants, which invariably causes the Fourier transform to favor the selection of narrow lines (slow relaxing) over broad signals (fast relaxing). As such, the PFG induced signal decay does not accurately represent

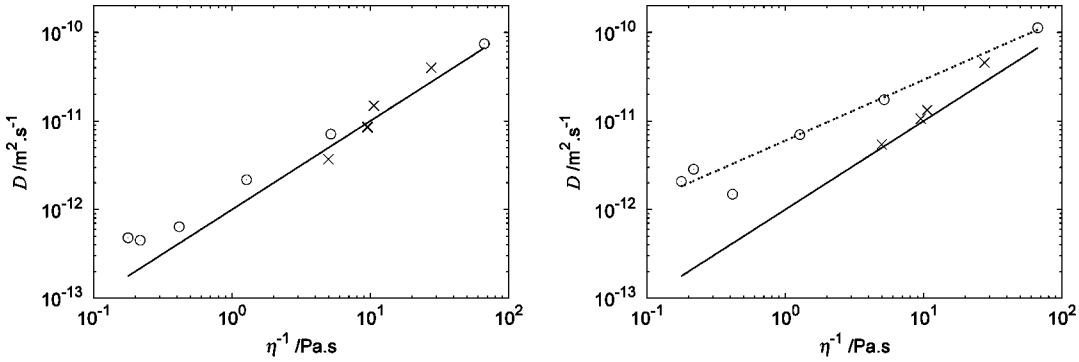

Figure 6. log−log plots of D as a function η^{-1} for 11 PIL from Table 1 at (a) 500 MHz and (b) 18.1 MHz. All PIL examined at 500 MHz followed the Stokes−Einstein equation (a). However, at 18.1 MHz the alcohol and alkoxy substituted amines (⊙) deviated from the equation whereas the alkylated amines (×) showed continuous Stokes−Einstein behavior (b). Errors were smaller than pointsize. The solid indicative line arises from fitting to the Stokes−Einstein equation. The dashed line in (b) arises from fitting to the fractional Stokes−Einstein equation (eq 6) with a fitting parameter of $\eta^{-0.69}$.

either much slower relaxing species (i.e., highly mobile ion diffusion that would attenuate the PFG signal quickly) or much faster species (i.e., liquid phase aggregates that give broad lines). However, at LF, an averaged value of all species was obtained due to the low spectral resolution and signal overlap. The field inhomogeneity of the NMR-MOUSE may also induce a shorter $T_{2\text{eff}}$. T_2 is a mixed effect in PIL at low field, and relaxation was facilitated by the NMR-MOUSE due to $1/T_{2\text{eff}} = 1/T_2 + f(\text{inhomegeneity})$, where f(inhomegeneity) is a factor induced by the magnetic field inhomogeneity of the NMR-MOUSE. The major contribution then comes from the faster relaxing species, which decay faster because of a shorter T_2. Therefore, the two magnetic field frequencies emphasized different assemblies of ions.

Self-diffusion coefficients at HF (D^{HF}) showed similar but not identical values for cation and anion, consistent with local ordering at the molecular level.[41] The Stokes−Einstein relation in a highly diluted solution relates the self-diffusion coefficient D to particles of radius r and the solvent viscosity η.

$$D = \frac{k_b T}{C\eta r_H} \tag{5}$$

where k_b = Boltzmann constant, T = absolute temperature, η = viscosity, r_H = hydrodynamic radius, C = constant whose value depends on the boundary conditions imposed on the surface of the particle (6π for so-called "stick" and 4π for "slip" boundary conditions).

Across the range of PIL examined, D^{HF} had a linear relationship to viscosity (η), indicating Stokes−Einstein behavior for the fast moving/slow relaxing ionic species (Figure 6a). The D at LF frequency changed most significantly for viscous PIL with slow diffusion, but less so for PIL with relatively fast diffusion (Table 1). Consistently, low field self-diffusion coefficients (D^{LF}) were slightly faster than either cation or anion at HF, yet both regimes followed an approximate trend of $D \propto \eta^{-1}$ (Figure 6). However, D^{LF} did not follow simple Stokes−Einstein behavior and deviated from a linear relationship to η^{-1} (Figure 6b). The viscous PIL containing $(HOEt)_2NH$ had self-diffusion coefficients almost an order of magnitude greater than that calculated from the Stokes−Einstein equation as opposed to the less viscous alkyl-substituted amines, which corresponded to η^{-1}, similar to the results from HF measurements.

TABLE 1: Self-Diffusion Coefficients at 500 and 18.1 MHz of PIL at 298 K ($D \times 10^{-12}$ m^2 s^{-1})

	500 MHz[a]			
protic ionic liquid	cation	anion	18.1 MHz[b]	η /Pa s
$(MeOEt)_2NH\cdot AcOH$	74.3	85.8	112.8	0.015
pyrr·AcOH	39.8	41.8	45.5	0.036
$Et_3N\cdot(BuO)_2PO_2H$	14.9	9.68	13.3	0.094
$Bu_3N\cdot(BuO)_2PO_2H$	8.63	9.13	10.61	0.105
pyrr·$(BuO)_2PO_2H$	8.45	7.85	10.57	0.105
$(MeOEt)_2NH\cdot MsOH$	7.18	8.21	17.38	0.193
$Et_2NH\cdot(BuO)_2PO_2H$	3.70	4.08	5.41	0.201
$(MeOEt)_2NH\cdot OSA$	2.17	2.17	7.01	0.785
$(HOEt)_2NH\cdot(BuO)_2PO_2H$[c]	0.64	0.51	1.49	2.41
$(HOEt)_2NH\cdot AcOH$[c]	0.48	0.60	2.08	5.65
$(HOEt)_2NH\cdot OSA$[c]	0.45	0.48	2.85	4.60

[a] g_{max} = 0.636 T m^{-1} unless indicated. ±5% estimated uncertainty based on the PGSTE standard deviation at 6 different big delta periods. [b] ±2% estimated uncertainty from nonlinear least-squares fitting. [c] g_{max} = 17.90 T m^{-1}.

The validity of the Stokes−Einstein approach in IL has been questioned due to the possibility of motional heterogeneities in regions where structure specific relaxation time can significantly differ from the average.[79] One of the hallmarks of a dynamic heterogeneity is a breakdown of the Stokes−Einstein relationship.[80−82] Deviations from eq 5 have been reported in supercooled water, glass forming liquids, concentrated protein solutions, colloids, polymer systems, and hydrogen bond forming liquids.[83−86] In the absence of a predictive theoretical model for deviation from the Stokes−Einstein relation, application of a fractional-Stokes−Einstein relationship (eq 6) can provide some information on specific changes in local molecular structure and ionic transport[87,88]

$$D = \frac{kT}{C\eta^{\xi} r_H} \tag{6}$$

where $0.5 < \xi < 0.95$ but commonly tends toward 0.8.[89]

An improved correlation of D^{LF} was obtained by fitting data to eq 6 (Figure 6). The obtained fitting parameter for fractional Stokes−Einstein behavior of $\xi = 0.69$ was within the expected range for network forming liquids.[89] When D^{LF} values of PIL were fit on the basis of a fractional Stokes−Einstein equation, there were fewer departures from the fitted line than the

corresponding Stokes−Einstein relationship (Figure 6b). Temperatures sufficiently greater than the PIL glass transition temperature and subsequent thermal disordering of aggregation may account for the D^{LF} results intermediate between eq 6 and eq 5 fitting (Figure 6b).[89] The slope of eq 6 only represents the range of examined PILs and deviations in ξ that would affect the region where the two equations intersect. The value for the PIL pyrr•AcOH was close to the eq 6 fit but did not show the change in diffusion coefficient observed for the alkoxy and hydroxy PILs at different magnetic fields. While not unique to the cation, since pyrr•$(BuO)_2PO_2H$ did not demonstrate a change, possibly an alternate diffusion mechanism contributed for pyrr•AcOH.

It has been hypothesized that Stokes−Einstein deviation is due primarily to the presence of transient mobile regions - particularly from dynamic structural heterogeneities.[90,91] Generally breakdown of the Stokes−Einstein equation can be characterized by specific contributions from different length scales, such as a short-range confinement to the cage of nearest neighbors followed by a persistent diffusion regime.[92,93] Structural heterogeneity in PIL has also been observed by controlled-stress rheometry where the long-range order was attributed to intermolecular hydrogen bonding susceptible to thermal disorder and molecular solvents.[62] The short-range interaction was completely disrupted when a further three water molecules inserted into the aggregates. For the low field diffusion measurements, PIL that deviated from Stokes−Einstein behavior all had hydrogen bonding groups distant from ionic moiety (i.e., −NH and −OH) (Table 1, Figure 6b). In particular, PIL containing MsOH, OSA, or $(HOEt)_2NH$ had multiple hydrogen bonding sites and are likely to form hydrogen bonded aggregates, hence, the large Stokes−Einstein deviations.

For the case of PIL diffusion, the difference in D between HF and LF likely arose from hydrogen bonded heterogeneity in the PIL structure that was emphasized by the difference in magnetic fields. The narrow lines seen at high field are related to species with longer T_2 relaxation times and, therefore, are not as sensitive to the relatively long PGSE sequence. At low field the lines are overlapped into a broad signal and, therefore, the signal of species with a larger D (broader lines) will dominate the signal following the PGSE sequence. Hence, measurements of the average D are, therefore, expected to be larger than at high field (as seen in Table 1). Magnetic field strength did not appreciably alter PIL structure, instead, the two fields emphasized the existence of a distribution of dynamic heterogeneous regions within PIL.

The picture that emerges from this discussion is of a highly associated liquid in which dynamics are restricted by the interactions with the surrounding ions and in which longer range motions could involve ion pairs and aggregates. To be effective in this respect, the aggregation need only be long enough lived to (not) contribute to the diffusion process. The aggregate may not necessarily have a lifetime longer than the characteristic relaxation time scale associated with diffusion, but the time fraction that each ion spends involved in these dynamic states must be significant on that time scale.

Conclusion

In this study, we report NMR relaxation and diffusion characterization of several protic ionic liquids at high and low magnetic fields. The dynamics of cations and anions were similar at both frequencies, indicating that the structure of PIL was not altered by the magnetic field frequency. High field diffusion revealed that the PIL cation and anion diffused as an ion pair. However, similar to aggretaion for aprotic IL, alkyl chain aggregation in PIL was not prevalent until the chain length exceeded four atoms from the ionic moiety.

Low field diffusion NMR showed evidence of deviation from Stokes−Einstein behavior, and a fractional Stokes−Einstein relation of $\xi = 0.69$ was found. Fractional Stokes−Einstein behavior did not manifest at high magnetic field frequency due mainly to the small amount of slow moving or high amount of slow relaxing species. The deviation was related to the formation of dynamic heterogeneity or aggregation within PIL and was most prominent for PIL with hydrogen bonding groups separated from ionic interactions. This suggests that in the steady state, PIL exists as networks of dynamic hydrogen bonded aggregates formed from the constituent ion pairs.

Acknowledgment. This work was supported by an ARC Linkage grant (LP0668123). We thank Prof. Bernhard Blümich (RWTH-Aachen) and Prof. William Price (University of Western Sydney) for instrument time and helpful discussions.

Supporting Information Available: DSC thermogram. This material is available free of charge via the Internet at http://pubs.acs.org.

References and Notes

(1) Rogers, R. D. *Nature* **2007**, *447*, 917–918.
(2) Plechkova, N. V.; Seddon, K. R. *Chem. Soc. Rev.* **2008**, *37*, 123–150.
(3) Swatloski, R. P.; Spear, S. K.; Holbrey, J. D.; Rogers, R. D. *J. Am. Chem. Soc.* **2002**, *124*, 4974–4975.
(4) Belieres, J.; Gervasio, D.; Angell, C. A. *Chem. Commun.* **2006**, 4799–4801.
(5) Abedin, S. Z. E.; Endres, F. *Acc. Chem. Res.* **2007**, *40*, 1106–1113.
(6) Armand, M.; Endres, F.; MacFarlane, D. R.; Ohno, H.; Scrosati, B. *Nat. Mater.* **2009**, *8*, 621–629.
(7) Borra, E. F.; Seddiki, O.; Angel, R.; Eisenstein, D.; Hickson, P.; Seddon, K. R.; Worden, S. P. *Nature* **2007**, *447*, 979–981.
(8) Bayley, P. M.; Lane, G. H.; Rocher, N. M.; Clare, B. R.; Best, A. S.; MacFarlane, D. R.; Forsyth, M. *Phys. Chem. Chem. Phys.* **2009**, *11*, 7202–7208.
(9) Canongia Lopes, J. N. A.; Padua, A. A. H. *J. Phys. Chem. B* **2006**, *110*, 3330–3335.
(10) Kraus, C. A. *J. Phys. Chem.* **1956**, *60*, 129–141.
(11) Seward, R. P. *J. Am. Chem. Soc.* **1951**, *73*, 515–517.
(12) Pitzer, K. S.; Simonson, J. M. *J. Am. Chem. Soc.* **1984**, *106*, 1973–1977.
(13) Schmuck, C.; Dudaczek, J. *Eur. J. Org. Chem.* **2007**, *2007*, 3326–3330.
(14) Bellachioma, G.; Ciancaleoni, G.; Zuccaccia, C.; Zuccaccia, D.; Macchioni, A. *Coord. Chem. Rev.* **2008**, *252*, 2224–2238.
(15) Ichikawa, T.; Yoshio, M.; Hamasaki, A.; Mukai, T.; Ohno, H.; Kato, T. *J. Am. Chem. Soc.* **2007**, *129*, 10662–10663.
(16) Tsuzuki, S.; Shinoda, W.; Saito, H.; Mikami, M.; Tokuda, H.; Watanabe, M. *J. Phys. Chem. B* **2009**, *113*, 10641–10649.
(17) Kornyshev, A. A. *J. Phys. Chem. B* **2007**, *111*, 5545–5557.
(18) Leal, J. P.; Esperança, J. M. S. S.; da Piedade, M. E. M.; Canongia Lopes, J. N.; Rebelo, L. P. N.; Seddon, K. R. *J. Phys. Chem. A* **2007**, *111*, 6176–6182.
(19) Atkin, R.; Warr, G. G. *J. Phys. Chem. C* **2007**, *111*, 5162–5168.
(20) Hayes, R.; Abedin, S. Z. E.; Atkin, R. *J. Phys. Chem. B* **2009**, *113*, 7049–7052.
(21) Canongia Lopes, J. N.; Costa Gomes, M. F.; Padua, A. A. H. *J. Phys. Chem. B* **2006**, *110*, 16816–16818.
(22) Wang, Y.; Voth, G. A. *J. Am. Chem. Soc.* **2005**, *127*, 12192–12193.
(23) Pott, T.; Meleard, P. *Phys. Chem. Chem. Phys.* **2009**, *11*, 5469–5475.
(24) Greaves, T. L.; Drummond, C. J. *Chem. Rev.* **2008**, *108*, 206–237.
(25) Yoshizawa, M.; Xu, W.; Angell, C. A. *J. Am. Chem. Soc.* **2003**, *125*, 15411–15419.
(26) Kennedy, D. F.; Drummond, C. J. *J. Phys. Chem. B* **2009**, *113*, 5690–5693.
(27) Atkin, R.; Warr, G. G. *J. Phys. Chem. B* **2008**, *112*, 4164–4166.
(28) Wakeham, D.; Hayes, R.; Warr, G. G.; Atkin, R. *J. Phys. Chem. B* **2009**, *113*, 5961–5966.
(29) Wang, F.; Izvekov, S.; Voth, G. A. *J. Am. Chem. Soc.* **2008**, *130*, 3120–3126.

(30) Umecky, T.; Saito, Y.; Okumura, Y.; Maeda, S.; Sakai, T. *J. Phys. Chem. B* **2008**, *112*, 3357–3364.
(31) Gutel, T.; Santini, C. C.; Padua, A. A. H.; Fenet, B.; Chauvin, Y.; Canongia Lopes, J. N.; Bayard, F.; Costa Gomes, M. F.; Pensado, A. S. *J. Phys. Chem. B* **2009**, *113*, 170–177.
(32) Hardacre, C.; Holbrey, J. D.; Nieuwenhuyzen, M.; Youngs, T. G. A. *Acc. Chem. Res.* **2007**, *40*, 1146–1155.
(33) Del Pöpolo, M. G.; Kohanoff, J.; Lynden-Bell, R. M.; Pinilla, C. *Acc. Chem. Res.* **2007**, *40*, 1156–1164.
(34) Fumino, K.; Wulf, A.; Ludwig, R. *Angew. Chem., Int. Ed.* **2009**, *48*, 3184–3186.
(35) Noda, A.; Hayamizu, K.; Watanabe, M. *J. Phys. Chem. B* **2001**, *105*, 4603–4610.
(36) Annat, G.; MacFarlane, D.; Forsyth, M. *J. Phys. Chem. B* **2007**, *111*, 9018–9024.
(37) Chung, S. H.; Lopato, R.; Greenbaum, S. G.; Shirota, H.; Castner, E. W.; Wishart, J. F. *J. Phys. Chem. B* **2007**, *111*, 4885–4893.
(38) Harris, K. R.; Kanakubo, M.; Tsuchihashi, N.; Ibuki, K.; Ueno, M. *J. Phys. Chem. B* **2008**, *112*, 9830–9840.
(39) Hayamizu, K.; Tsuzuki, S.; Seki, S.; Ohno, Y.; Miyashiro, H.; Kobayashi, Y. *J. Phys. Chem. B* **2008**, *112*, 1189–1197.
(40) Judeinstein, P.; Iojoiu, C.; Sanchez, J.; Ancian, B. *J. Phys. Chem. B* **2008**, *112*, 3680–3683.
(41) Castiglione, F.; Moreno, M.; Raos, G.; Famulari, A.; Mele, A.; Appetecchi, G. B.; Passerini, S. *J. Phys. Chem. B* **2009**, *113*, 10750–10759.
(42) Valentini, M.; Pregosin, P. S.; Ruegger, H. *J. Chem. Soc., Dalton Trans.* **2000**, 4507–4510.
(43) Price, W. S. *Aust. J. Chem.* **2003**, *56*, 855–860.
(44) Pregosin, P. S. *Prog. Nucl. Magn. Reson. Spectrosc.* **2006**, *49*, 261–288.
(45) Menjoge, A.; Dixon, J.; Brennecke, J. F.; Maginn, E. J.; Vasenkov, S. *J. Phys. Chem. B* **2009**, *113*, 6353–6359.
(46) Kataoka, H.; Saito, Y. *J. Phys. Chem. B* **2002**, *106*, 13064–13068.
(47) Kataoka, H.; Saito, Y.; Sakai, T.; Deki, S.; Ikeda, T. *J. Phys. Chem. B* **2001**, *105*, 2546–2550.
(48) Holstein, P.; Bender, M.; Galvosas, P.; Geschke, D.; Kärger, J. *J. Magn. Reson.* **2000**, *143*, 427–430.
(49) English, N. J.; Mooney, D. A. *J. Phys. Chem. B* **2009**, *113*, 10128–10134.
(50) Umecky, T.; Saito, Y.; Matsumoto, H. *J. Phys. Chem. B* **2009**, *113*, 8466–8468.
(51) Saito, Y.; Hirai, K.; Murata, S.; Kishii, Y.; Kii, K.; Yoshio, M.; Kato, T. *J. Phys. Chem. B* **2005**, *109*, 11563–11571.
(52) Martin, S. M.; Yonezawa, J.; Horner, M. J.; Macosko, C. W.; Ward, M. D. *Chem. Mater.* **2004**, *16*, 3045–3055.
(53) Wang, Y. *J. Phys. Chem. B* **2009**, *113*, 11058–11060.
(54) Gao, S.; Chapman, W. G.; House, W. *J. Magn. Reson.* **2009**, *197*, 208–212.
(55) Metais, A.; Mariette, F. *J. Magn. Reson.* **2003**, *165*, 265–275.
(56) Maus, A.; Hertlein, C.; Saalwächter, K. *Macromol. Chem. Phys.* **2006**, *207*, 1150–1158.
(57) Schmidt-Rohr, K.; Spiess, H. W. *Multidimensional Solid-State NMR and Polymers*; Academic Press: San Diego, 1994.
(58) Mellinger, F.; Wilhelm, M.; Spiess, H. W. *Macromolecules* **1999**, *32*, 4686–4691.
(59) Le Botlan, D. J.; Ouguerram, L. *Anal. Chim. Acta* **1997**, *349*, 339–347.
(60) Burrell, G. L.; Burgar, I. M.; Separovic, F.; Dunlop, N. F. *Phys. Chem. Chem. Phys.* **2010**, *12*, 1571–1577.
(61) Rata, D.; Casanova, F.; Perlo, J.; Demco, D.; Blmich, B. *J. Magn. Reson.* **2006**, *180*, 229–235.
(62) Burrell, G. L.; Dunlop, N. F.; Separovic, F. *Soft Matter* **2010**, 2080–2086.
(63) Derome, A. E. *Modern Nmr Techniques for Chemistry Research*; Pergamon: Oxford, 1987.
(64) Price, W. S.; Hayamizu, K.; Ide, H.; Arata, Y. *J. Magn. Reson.* **1999**, *139*, 205–212.
(65) Stejskal, E. O.; Tanner, J. E. *J. Chem. Phys.* **1965**, *42*, 288–292.
(66) Ando, I.; Asakura, T. *Solid State NMR of Polymers*; Elsevier, Amsterdam, 1998.
(67) Wang, C. K.; Schirra, H. J.; Craik, D. J. *PLoS ONE* **2008**, *3*, e3820.
(68) Zhao, C.; Burrell, G.; Torriero, A. A. J.; Separovic, F.; Dunlop, N. F.; MacFarlane, D. R.; Bond, A. M. *J. Phys. Chem. B* **2008**, *112*, 6923–6936.
(69) Cornell, B.; Davenport, J.; Separovic, F. *BBA-Biomembranes* **1982**, *689*, 337–345.
(70) Abragam, A. *Principles of Nuclear Magnetism*; Oxford University Press, Inc.: New York, 1983.
(71) Zhao, Y.; Gao, S.; Wang, J.; Tang, J. *J. Phys. Chem. B* **2008**, *112*, 2031–2039.
(72) Bakhmutov, V. I. *Practical NMR relaxation for chemists*; John Wiley and Sons: Chichester, U.K., 2004.
(73) Mustarelli, P.; Capiglia, C.; Quartarone, E.; Tomasi, C.; Ferloni, P. *Phys. Rev. B* **1999**, *60*, 7228–7233.
(74) Mortimer, M.; Moore, E. A.; Williams, M. A. K. *J. Chem. Soc., Faraday Trans.* **1996**, *92*, 5043–5046.
(75) Donoso, J. P.; Bonagamba, T. J.; Panepucci, H. C.; Oliveira, L. N.; Gorecki, W.; Berthier, C.; Armand, M. *J. Chem. Phys.* **1993**, *98*, 10026–10036.
(76) Hapiot, P.; Lagrost, C. *Chem. Rev.* **2008**, *108*, 2238–2264.
(77) Saito, Y.; Hirai, K.; Matsumoto, K.; Hagiwara, R.; Minamizaki, Y. *J. Phys. Chem. B* **2005**, *109*, 2942–2948.
(78) Calculator Plugins were used for structure property prediction and calculation, *Marvin 5.3.2* **2010**, ChemAxon (http://www.chemaxon.com).
(79) Köddermann, T.; Ludwig, R.; Paschek, D. *ChemPhysChem* **2008**, *9*, 1851–1858.
(80) Eaves, J. D.; Reichman, D. R. *Proc. Natl. Acad. Sci.* **2009**, *106*, 15171–15175.
(81) Jung, Y.; Garrahan, J. P.; Chandler, D. *Phys. Rev. E* **2004**, *69*, 061205.
(82) Jung, Y.; Garrahan, J. P.; Chandler, D. *J. Chem. Phys.* **2005**, *123*, 084509−10.
(83) Mallamce, F.; Broccio, M.; Corsaro, C.; Faraone, A.; Liu, L.; Mou, C.; Chen, S. *J. Phys. Condens. Matter* **2006**, *18*, S2285–S2297.
(84) Angell, C. A. *Science* **1995**, *267*, 1924–1935.
(85) Chirico, G.; Placidi, M.; Cannistraro, S. *J. Phys. Chem. B* **1999**, *103*, 1746–1751.
(86) Fernandez-Alonso, F.; Bermejo, F. J.; McLain, S. E.; Turner, J. F. C.; Molaison, J. J.; Herwig, K. W. *Phys. Rev. Lett.* **2007**, *98*, 077801−4.
(87) Xu, L.; Mallamace, F.; Yan, Z.; Starr, F. W.; Buldyrev, S. V.; Stanley, H. E. *Nat. Phys.* **2009**, *5*, 565–569.
(88) Voronel, A.; Veliyulin, E.; Machavariani, V. S.; Kisliuk, A.; Quitmann, D. *Phys. Rev. Lett.* **1998**, *80*, 2630.
(89) Becker, S. R.; Poole, P. H.; Starr, F. W. *Phys. Rev. Lett.* **2006**, *97*, 055901−4.
(90) Ediger, M. D. *Annu. Rev. Phys. Chem.* **2000**, *51*, 99–128.
(91) Lubchenko, V.; Wolynes, P. G. *Annu. Rev. Phys. Chem.* **2007**, *58*, 235–266.
(92) Puertas, A. M.; Michele, C. D.; Sciortino, F.; Tartaglia, P.; Zaccarelli, E. *J. Chem. Phys.* **2007**, *127*, 144906–10.
(93) Krekelberg, W. P.; Mittal, J.; Ganesan, V.; Truskett, T. M. *J. Chem. Phys.* **2007**, *127*, 044502−8.

JP105087N